Dalton Transactions

ROYAL SOCIETY OF CHEMISTRY

PAPER

View Article Online
View Journal

Cite this: DOI: 10.1039/d6dt00405a

Structure–activity relationships of morpholine-modified silicon(IV) phthalocyanines as potential antidiabetic agents

Turgut Keleş,[a,b] Zekeriya Biyiklioglu, *[c] Gökçe Seyhan[d,e] and Burak Barut[d]

Type 2 diabetes mellitus (DM) is a chronic metabolic disorder with a rapidly increasing global prevalence, highlighting the need for safer and more effective therapeutic strategies. In this study, a series of axially disubstituted silicon(IV) phthalocyanines bearing morpholine functional groups and their water-soluble derivatives were synthesized, structurally characterized, and evaluated for their antidiabetic potential. The synthesized compounds were characterized by FT-IR, ^{1}H and ^{13}C NMR, UV–Vis spectroscopy, and mass spectrometry. The *in vitro* antidiabetic activity of the compounds was evaluated through α-glycosidase and α-amylase inhibition assays. The non-ionic silicon(IV) phthalocyanine derivatives **MT-C3-H-Si** and **MT-C3-D-Si** exhibited strong α-glucosidase inhibitory activity with IC_{50} values of 16.02 ± 0.94 μM and 44.14 ± 4.06 μM, respectively, showing higher potency than the standard inhibitor acarbose (IC_{50} = 60.51 ± 4.66 μM). In contrast, the water-soluble derivatives **MT-C3-H-SiQ** and **MT-C3-D-SiQ** displayed lower inhibitory activity (IC_{50} = 68.80 ± 5.12 μM and >100 μM, respectively), indicating that increased hydrophilicity does not necessarily enhance enzyme inhibition. All compounds exhibited weak α-amylase inhibition (IC_{50} > 100 μM) compared with acarbose (IC_{50} = 25.29 ± 3.50 μM). Kinetic studies revealed that **MT-C3-H-Si** and **MT-C3-D-Si** inhibit α-glycosidase *via* a non-competitive mechanism, with K_i values of 9.45 ± 1.45 μM and 29.06 ± 5.16 μM, respectively. This is characterized by decreased V_{max} values without significant changes in K_m, suggesting interaction with allosteric regions of the enzyme. Overall, these findings highlight axially disubstituted silicon(IV) phthalocyanines as promising molecular scaffolds and contribute valuable insight into the limited literature on their antidiabetic enzyme inhibition properties.

Received 15th February 2026,
Accepted 9th April 2026

DOI: 10.1039/d6dt00405a

rsc.li/dalton

1. Introduction

Diabetes mellitus (DM) is a multifactorial metabolic disease characterized by chronic hyperglycemia. Hyperglycemia occurs when the secretion or action of insulin is deficient. Due to its relationship with insulin, DM affects adipose tissues, skeletal muscles, and the liver. In diabetic patients, it presents with symptoms such as increased polyphagia, polydipsia, polyuria, weight loss, and visual impairment.[1,2] If left untreated, the disease progresses and may lead to severe complications including blindness, cardiovascular disease, stroke, and renal dysfunction.[3] According to the International Diabetes Federation, in 2021, approximately 540 million adults had DM, which is projected to reach approximately 640 million in 2030 and 790 million in 2045. Therefore, health expenditures for this disease are quite high. Health expenditures, which were $966 billion in 2021, are expected to reach $1054 billion in 2045.[4]

DM is a major global health concern, and although there is no definitive cure, it can be effectively managed. Blood glucose levels can be controlled through insulin therapy, pharmacological agents, and lifestyle modifications, including diet and physical activity. Type 1 and Type 2 DM are the most common types of DM.[5] Among these, Type 2 DM accounts for approximately 90% of all cases and is characterized by impaired insulin secretion due to pancreatic β-cell dysfunction and decreased insulin sensitivity resulting from abnormalities in insulin receptors.[6] One of the key therapeutic strategies for managing Type 2 DM involves the inhibition of carbohydrate-digesting enzymes. In this context, α-glycosidase and α-amylase enzymes have attracted considerable attention as

[a]*Karadeniz Technical University, Graduate School of Natural and Applied Science, Trabzon, Türkiye*
[b]*Central Research Laboratory Application and Research Center, Recep Tayyip Erdogan University, Rize, Turkey*
[c]*Karadeniz Technical University, Faculty of Science, Department of Chemistry, Trabzon, Türkiye. E-mail: zekeriyab@ktu.edu.tr; Fax: +90 462 325 31 96; Tel: +90462 377 36 64*
[d]*Karadeniz Technical University, Faculty of Pharmacy, Department of Biochemistry, Trabzon, Türkiye*
[e]*Karadeniz Technical University, Graduate School of Health Sciences, Department of Biochemistry (Pharmacy), Trabzon, Türkiye*

important targets in drug development. α-Glycosidase plays a critical role in the hydrolysis of α-(1,6)-D-glycosidic bonds, facilitating the breakdown of complex carbohydrates into absorbable monosaccharides. Inhibition of this enzyme helps regulate postprandial hyperglycemia without directly affecting insulin secretion.[7] Similarly, α-amylase catalyzes the hydrolysis of α-(1,4)-D-glycosidic bonds, contributing to starch digestion.[8] Clinically used inhibitors such as acarbose, miglitol, and voglibose are effective; however, they are often associated with gastrointestinal side effects, including flatulence, abdominal discomfort, and bloating. These adverse effects are primarily attributed to the strong inhibition of α-amylase and α-glycosidase, leading to the fermentation of undigested carbohydrates.[9,10] Therefore, the development of novel inhibitors that provide enhanced efficacy, minimal adverse effects, and strong α-glycosidase and mild α-amylase inhibition remains an important research objective.

In the mid-twentieth century, significant progress was made in the development of new macroheterocyclic compounds through the incorporation of different elements into the phthalocyanine core.[11]

Like closely related porphyrin analogues, phthalocyanines have an 18π-electron conjugated system. However, unlike porphyrins, they contain imine bridges and isoindole units instead of methine bridges and pyrrole rings.[12] These structural differences result in strong absorption in the red and near-infrared (NIR) region, typically 700 nm.[13] Despite these advantageous optical properties, the application of phthalocyanines is often limited by their poor solubility and strong tendency to aggregate due to π–π stacking interactions.[14] To overcome these limitations, various structural modification strategies have been developed, including the introduction of substituents and metal ions into the macrocyclic core to improve solubility, reduce aggregation, and enhance synthetic accessibility.[15] Among metal phthalocyanines, silicon(IV) phthalocyanines have attracted particular interest due to their unique hexacoordinated structure and remarkable stability of Si–N bonds.[16] Additionally, the presence of two unique axial positions that can be easily functionalized provides a significant advantage over conventional phthalocyanines. Bulky or polar substituents introduced at these axial positions are more effective than α- or β-substituted phthalocyanines, as they disrupt intermolecular interactions and reduce planarity.[17] In addition, axial Si–O and Si–C bonds have enabled a wide range of applications in biomedical fields due to their stability, cost-effective synthesis, and low toxicity.[18] In particular, in biological systems, silicon(IV) phthalocyanines exhibit improved performance compared to peripheral and non-peripheral metal phthalocyanines, as axial ligands increase the distance between macrocycles, thereby reducing aggregation and intermolecular interactions.[19]

Furthermore, water-soluble silicon(IV) phthalocyanines can be readily obtained *via* simple quaternization of nitrogen atoms in axially substituted groups with methyl iodide. These ionic derivatives are considered promising candidates for biological applications, particularly as enzyme inhibitors in metabolic diseases. Several studies have investigated the biological activity of silicon(IV) phthalocyanines. For example, Solğun *et al.* synthesized axially disubstituted bis-(3,4,5-trimethoxybenzyloxy)silicon(IV) phthalocyanine. The antidiabetic activity of the compound was investigated at concentrations of 100, 200 and 400 mg L^{-1} and 22.66%, 29.16% and 41.66% enzyme inhibition was recorded, respectively.[20] In another study, Çelik *et al.* investigated the α-amylase and α-glycosidase enzyme inhibition activities of silicon(IV) phthalocyanines (**6a** and **6b**) containing 1,2,3-triazole Schiff base groups.[21] Compound **6a** showed very little inhibition against α-amylase, while it did not inhibit α-glucosidase. However, **6b** showed moderate inhibition against α-amylase, while α-glucosidase showed about 8 times more effective inhibition compared to acarbose. The presence of electron-releasing methoxy groups in compound **6b** may have led to the increase in the activity. In a similar study, Yalazan *et al.* designed axially disubstituted silicon(IV) phthalocyanines with geraniol and phytol groups, which are acyclic hydrocarbons. The α-glycosidase inhibitory effects of silicon(IV) phthalocyanines were tested using spectrophotometric assays. These compounds had lower α-glycosidase inhibition activity compared to acarbose.[22] Overall, studies on the α-glycosidase and α-amylase enzyme inhibition activities of silicon(IV) phthalocyanines remain limited, highlighting the need for further investigation in this area.

Therefore, one of the aims of this study was to design and develop new silicon(IV) phthalocyanines and investigate their activities against these enzymes. On the other hand, the potential of these new silicon(IV) phthalocyanine compounds as drug candidates for the treatment of DM has been evaluated.

In this study, axially disubstituted silicon(IV) phthalocyanines containing morpholine groups and their water-soluble derivatives were synthesized and characterized using NMR, FT-IR, UV-Vis and MS spectroscopic techniques. Afterwards, the α-glycosidase and α-amylase enzyme inhibition activities of these compounds were investigated. Inhibition activities, kinetic tests, inhibition types and inhibition constants of these compounds were reported in detail.

2. Materials and methods

All solvents and reagents used in the reactions were of reagent grade quality and were obtained from commercial suppliers. Also, the materials, equipment, *in vitro* α-glycosidase and α-amylase inhibition assays, kinetic and statistical analysis experimental data are given in the SI.

2.1. The synthesis of 4-(3-(3-chloropropoxy)phenyl) morpholine (MT-C3-Cl)

In a 250 mL double-necked flask, 1 g (5.60 mmol) of 3-(4-morphonyl)phenol and 200 mg (8.40 mmol) of NaH in 10 mL of dry DMF were stirred at 0 °C to −5 °C under a nitrogen gas atmosphere for 1 hour. To this mixture, 0.60 mL (5.60 mmol) of 1-bromo-3-chloropropane in 3 mL dry DMF was slowly added using a dropping funnel. The reaction mixture was

stirred at room temperature under a nitrogen gas atmosphere for 1 day. At the end of the time, the contents of the flask were poured into an ice-water mixture, 50 mL of chloroform was added and the reaction mixture was stirred for 1 day. The crude product was then extracted 3 times with a chloroform/water mixture. The chloroform was then evaporated under reduced pressure and the crude product was purified from the column loaded with aluminum oxide, using chloroform as the mobile phase. Yield: 650 mg (46%). IR (ATR), $\bar{\nu}_{max}/cm^{-1}$: 3095–3031 (Ar–H), 2962–2824 (Aliph. C–H), 1600, 1496, 1450, 1382, 1304, 1257, 1192, 1122, 1051, 993, 877, 835, 759, 687, 651. ^{1}H-NMR (DMSO-d_6), (δ: ppm): 7.10 (t, 1H, Ar–H), 6.52 (d, 1H, Ar–H), 6.45 (s, 1H, Ar–H), 6.40 (d, 1H, Ar–H), 4.03 (t, 2H, Ar–O–CH_2), 3.76 (t, 2H, CH_2–Cl), 3.70 (t, 4H, CH_2–O), 3.06 (t, 4H, CH_2–N), 2.15–2.09 (m, 2H, –CH_2–).^{13}C-NMR (DMSO-d_6), (δ: ppm): 159.75, 152.91, 130.11, 108.35, 105.35, 102.23, 66.52, 64.42, 48.82, 42.47, 32.24. LC/MS (ESI) m/z: 256.210 $[M]^+$.

2.2. The synthesis of (4-(3-(3-morpholinophenoxy)propoxy) phenyl)methanol (MT-C3-H-OH)

In a 250 mL flask, 315 mg (2.53 mmol) of 4-hydroxybenzylalcohol and 2.4 g (17.70 mmol) of dry K_2CO_3 were dissolved in 60 mL acetone. To the reaction mixture, 650 mg (2.53 mmol) of 4-(3-(3-chloropropoxy)phenyl)morpholine (**MT-C3-Cl**) and 528 mg (2 mmol) of 18-crown-6 were added and stirred at 70 °C under a nitrogen atmosphere for 2 days. The reaction was cooled to room temperature, filtered through black band filter paper and the solvent was evaporated. The crude product obtained was extracted 3 times with a chloroform/water mixture. The solvent of the organic phase was completely evaporated and the crude product was purified with chloroform through a neutral silica gel-loaded column. Yield: 380 mg (44%), melting point: 85–87 °C. IR (ATR), $\bar{\nu}_{max}/cm^{-1}$: 3426 (–OH), 3051 (Ar. C–H), 2967–2837 (Aliph. C–H), 1614, 1576, 1512, 1448, 1393, 1301, 1266, 1240, 1196, 1113, 1042, 963, 876, 837, 745, 680. ^{1}H-NMR (DMSO-d_6), (δ: ppm): 7.21 (d, 2H, Ar–H), 7.09 (t, 1H, Ar–H), 6.89 (d, 2H, Ar–H), 6.51 (d, 1H, Ar–H), 6.45 (s, 1H, Ar–H), 6.40 (d, 2H, Ar–H),4.39 (s, 2H, CH_2–OH), 4.08 (t, 4H, Ar–O–CH_2), 3.70 (t, 4H, CH_2–O), 3.06 (t, 4H, CH_2–N), 2.13–2.10 (m, 2H, –CH_2–).^{13}C-NMR (DMSO-d_6), (δ: ppm): 159.88, 157.80, 152.87, 135.04, 130.10, 128.34, 114.48, 108.27, 105.47, 102.24, 66.51, 64.61, 64.43, 62.97, 48.85, 29.20. LC/MS (ESI) m/z: 344.310 $[M + H]^+$.

2.3. The synthesis of (3,5-bis(3-(3-morpholinphenoxy) propoxy)phenyl)methanol (MT-C3-D-OH)

MT-C3-D-OH was synthesized similarly to **MT-C3-H-OH**. 3,5-Dihydroxybenzyl alcohol was used instead of 4-hydroxybenzyl alcohol. Yield: 400 mg (55%). IR (ATR), $\bar{\nu}_{max}/cm^{-1}$: 3437 (–OH), 3092–3035 (Ar–H), 2963–2830 (Aliph. C–H), 1598, 1497, 1450, 1383, 1266, 1193, 1163, 1119, 1066, 996, 834, 760, 688. ^{1}H-NMR (DMSO-d_6), (δ: ppm): 7.09 (t, 2H, Ar–H), 6.48 (t, 6H, Ar–H), 6.37 (t, 3H, Ar–H), 4.39 (s, 2H, CH_2–OH), 4.06 (t, 8H, Ar–O–CH_2), 3.68 (t, 8H, CH_2–O), 3.05 (t, 8H, CH_2–N), 2.11–2.08 (m, 4H, –CH_2–). ^{13}C-NMR (DMSO-d_6), (δ: ppm): 159.97, 159.87, 152.90, 145.64, 130.09, 108.25, 105.42, 105.09, 102.19, 99.86, 66.51, 64.60, 64.39, 63.22, 48.83, 29.17. MALDI-TOF-MS m/z: 578.038 $[M]^+$.

2.4. The synthesis of silicon(IV) phthalocyanine compound (MT-C3-H-Si)

In a 50 mL flask, 120 mg (0.35 mmol) of (4-(4-(3-(3-morpholinphenoxy)propoxy)phenyl)phenyl)methanol (**MT-C3-H-OH**) was dissolved in 10 mL of dry toluene and 100 mg (0.16 mmol) of silicon phthalocyanine dichloride was added and stirred under a nitrogen atmosphere for 10 minutes. Then 8.40 mg (0.35 mmol) sodium hydride was added to the reaction medium and the mixture was stirred at 110 °C for one day. At the end of the time, the mixture was cooled to room temperature and the solvent was removed by evaporation. The crude product was purified from the neutral silica gel loaded column using chloroform as the mobile phase. Yield: 45 mg (18%), m.p.: >250 °C. IR (ATR), $\bar{\nu}_{max}/cm^{-1}$: 3069 (Ar–H), 2964–2855 (Aliph. C–H), 1600, 1507, 1429, 1335, 1291, 1242, 1193, 1167, 1121, 1077, 908, 759, 731, 680. ^{1}H-NMR ($CDCl_3$), (δ: ppm): 9.58 (m, 8H, Pc-H_α), 8.31 (m, 8H, Pc-H_β), 7.14 (t, 4H, Ar–H), 6.51 (d, 4H, Ar–H), 6.40 (s, 4H, Ar–H), 5.68 (d, 4H, Ar–H), 4.24 (t, 4H, –Ar–O–CH_2)$_\mathbf{b}$, 3.96 (s, 4H, Ar–O–CH_2)$_\mathbf{d}$, 3.81 (t, 8H, CH_2–O)$_\mathbf{f}$, 3.11 (t, 8H, CH_2–N)$_\mathbf{e}$, 2.00 (m, 4H, –CH_2–)$_\mathbf{c}$, −0.78 (s, 4H, Si–O–CH_2)$_\mathbf{a}$. ^{13}C-NMR ($CDCl_3$), (δ: ppm): 159.87, 156.17, 152.65, 149.28, 136.03, 131.29, 130.68, 129.81, 124.59, 123.55, 112.55, 108.46, 105.35, 102.63, 66.85, 64.30, 63.98, 57.42, 49.24, 29.10. UV-Vis (DMF) λ_{max} nm (log ε): 678 (5.04), 650 (4.29), 612 (4.33), 332 (4.66). MALDI-TOF-MS m/z: 1225.105 $[M]^+$.

2.5. The synthesis of silicon(IV) phthalocyanine compound (MT-C3-D-Si)

MT-C3-D-Si phthalocyanine was synthesized similarly to **MT-C3-H-Si** phthalocyanine with minor modification, using (3,5-bis(3-(3-morpholinophenoxy)propoxy)phenyl)methanol (**MT-C3-D-OH**) instead of **MT-C3-H-OH**. The crude product was purified from the neutral silica gel loaded column using chloroform as the mobile phase. Yield: 60 mg (22%), m.p.: >250 °C. IR (ATR), $\bar{\nu}_{max}/cm^{-1}$: 3081 (Ar–H), 2960–2860 (Aliph. C–H), 1597, 1496, 1450, 1336, 1260, 1192, 1162, 1121, 1066, 996, 832, 757, 738, 688. ^{1}H-NMR ($CDCl_3$), (δ: ppm): 9.57 (m, 8H, Pc-H_α), 8.27 (m, 8H, Pc-H_β), 7.18 (t, 6H, Ar–H), 6.53 (d, 6H, Ar–H), 6.43 (t, 8H, Ar–H), 5.50 (s, 2H, Ar–H), 3.85 (t, 8H, Ar–O–CH_2)$_b$, 3.83 (d, 16H, CH_2–O)$_f$, 3.17 (t, 8H, Ar–O–CH_2)$_d$, 3.12 (t, 16H, CH_2–N)$_e$, 1.84 (m, 8H, –CH_2–)$_c$, −0.72 (s, 4H, Si–O–CH_2)$_a$. ^{13}C-NMR ($CDCl_3$), (δ: ppm): 159.87, 158.27, 152.66, 149.37, 141.45, 135.99, 130.78, 129.82, 123.54, 108.46, 105.45, 102.68, 101.21, 99.20, 66.86, 64.34, 63.42, 58.16, 49.28, 29.05. UV-Vis (DMF) λ_{max} nm (log ε): 681 (5.00), 648 (4.26), 615 (4.30), 335 (4.65). MALDI-TOF-MS m/z: 1695.166 $[M]^+$.

2.6. The general method for the synthesis of water-soluble silicon(IV) phthalocyanines

20 mg (0.016 mmol) of **MT-C3-H-Si** and **MT-C3-D-Si** were dissolved separately in 2.50 mL of chloroform and 2 mL of iodomethane was added to these mixtures. The reaction mixtures were stirred at room temperature in the dark for 6 days. At the

end of the time, the precipitated part was filtered through a glass crucible. The unreacted portion was washed with chloroform and diethylether and removed from the medium. The obtained portion was dried *in vacuo*.

2.6.1. The synthesis of MT-C3-H-SiQ. Yield: 15 mg (61%), m.p.: >300 °C. IR (ATR), $\bar{\nu}_{max}/cm^{-1}$: 3056 (Ar–H), 2932–2807 (Aliph. C–H), 1612, 1519, 1469, 1429, 1337, 1290, 1166, 1119, 1067, 911, 830, 759, 727. UV-Vis (DMF) λ_{max} nm (log ε): 668 (5.04), 643 (4.63), 604 (4.35), 355 (4.88). MALDI-TOF-MS *m*/*z*: 682.570 $[M - 2I + 3H_2O + H]^{2+}$.

2.6.2. The synthesis of MT-C3-D-SiQ. Yield: 10 mg (38%), m.p.: >300 °C. IR (ATR), $\bar{\nu}_{max}/cm^{-1}$: 3060 (Ar–H), 2985–2881 (Aliph. C–H), 1610, 1519, 1471, 1425, 1332, 1287, 1167, 1119, 1064, 910, 832, 757, 729. UV-Vis (DMF) λ_{max} nm (log ε): 668 (5.03), 643 (4.33), 604 (4.35), 355 (4.60). MALDI-TOF-MS *m*/*z*: 440.849 $[M - 4I + H]^{4+}$.

3. Results and discussion

3.1. Synthesis and characterization

Scheme 1 illustrates the synthetic route for morpholine-substituted silicon(IV) phthalocyanines (**MT-C3-H-Si** and **MT-C3-D-Si**) and their water-soluble derivatives (**MT-C3-H-SiQ** and **MT-C3-D-SiQ**). Initially, the **MT-C3-Cl** compound was synthesized *via* a nucleophilic substitution reaction between 3-morpholine phenol and 1-bromo-3-chloropropane in DMF using NaH as a base.

The synthesized ligand precursor **MT-C3-Cl** was characterized by FT-IR, NMR, and ESI-MS techniques to confirm its molecular structure. In the IR spectrum of **MT-C3-Cl**, aromatic C–H stretching vibrations were observed at 3095–3031 cm^{-1}, while aliphatic C–H stretching bands appeared at 2962–2824 cm^{-1}, indicating the presence of both aromatic and aliphatic moieties in the molecule. The characteristic aromatic C=C stretching band was detected at 1600 cm^{-1}, supporting the presence of the aromatic ring system. In addition, the C–O–C and C–N–C stretching vibrations observed at 1257 and 1122 cm^{-1}, respectively, are characteristic of the morpholine ring and confirm the presence of the ether and tertiary amine functionalities associated with the morpholine moiety in the proposed structure (Fig. S1). The ^{1}H NMR spectrum (DMSO-d_6) of **MT-C3-Cl** exhibited four aromatic protons in the range of 7.10–6.40 ppm, which correspond to the protons on the substituted aromatic ring. The fourteen aliphatic protons observed between 4.03 and 2.15 ppm are attributed to the methylene groups associated with the morpholine and propyl fragments (Fig. S2a). In the ^{13}C NMR spectrum, aromatic carbon signals were observed in the range of 159.75–102.23 ppm, while aliphatic carbons appeared at 66.52 (CH_2–O), 64.42 (Ar–O–CH_2), 48.82 (CH_2–N), 42.47 (CH_2–Cl), and 32.24 ppm (–CH_2–), supporting the structural integrity of the compound (Fig. S2b). Notably, the signal at 42.47 ppm is characteristic of a C–Cl carbon environment, whereas C–Br carbons are typically observed at lower chemical shift values (*ca.* 30–40 ppm). This observation indicates that the substitution occurred *via* bromide displacement, resulting in the formation of the chlorine-containing product, in agreement with the literature reports.[23,24] The ESI-MS spectrum further supports the proposed structure, showing a molecular ion peak at *m*/*z* = 256.21 corresponding to the protonated molecule M + H^+ (Fig. S3). In addition, a signal at *m*/*z* = 298.21 was detected and carefully evaluated. Detailed inspection of the magnified spectrum revealed that this peak does not exhibit the characteristic isotopic pattern of bromine (M/M + 2 doublet with approximately 1 : 1 intensity for ^{79}Br/^{81}Br).[25] Therefore, the presence of a brominated species can be excluded. Instead, this signal is attributed to a solvent-derived adduct, most likely, which is com-

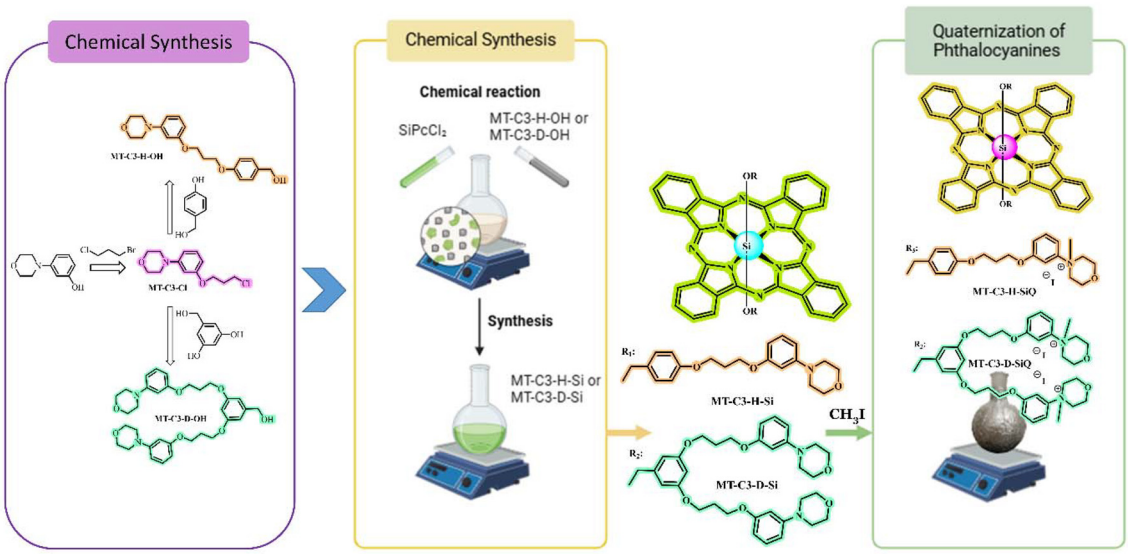

Scheme 1 Synthetic route for the preparation of axially disubstituted silicon(IV) phthalocyanines (**MT-C3-H-Si** and **MT-C3-D-Si**) and their water-soluble derivatives (**MT-C3-H-SiQ** and **MT-C3-D-SiQ**).

monly observed in ESI-MS analyses. Subsequently, **MT-C3-H-OH** and **MT-C3-D-OH** were synthesized *via* nucleophilic substitution of **MT-C3-Cl** with 4-hydroxybenzyl alcohol and 3,5-dihydroxybenzyl alcohol, respectively, in acetone using K_2CO_3 as a base. This reaction pathway enables the introduction of hydroxybenzyl substituents through a nucleophilic displacement of the chlorine atom, leading to the formation of ether-linked derivatives.

The IR spectra of both **MT-C3-H-OH** and **MT-C3-D-OH** confirmed the successful substitution reaction. In particular, the appearance of broad O–H stretching bands at 3426 cm^{-1} for **MT-C3-H-OH** and 3437 cm^{-1} for **MT-C3-D-OH** clearly indicates the presence of hydroxyl groups in the molecular structures. Aromatic C–H stretching bands were observed at 3051 cm^{-1} for **MT-C3-H-OH** and 3092–3035 cm^{-1} for **MT-C3-D-OH**, while aliphatic C–H stretching vibrations appeared in the ranges of 2967–2837 cm^{-1} and 2963–2830 cm^{-1}, respectively, which are consistent with the coexistence of aromatic and aliphatic fragments within the ligands (Fig. S4 and S7). The ^{1}H NMR spectrum of **MT-C3-H-OH** (DMSO-d_6) displayed aromatic proton signals between 7.21 and 6.40 ppm and aliphatic proton signals between 4.39 and 2.10 ppm, which are consistent with the expected proton environments of the substituted benzyl, morpholine and alkyl units (Fig. S5a). The ^{13}C NMR spectrum showed sixteen carbon signals within the range of 159.88–29.20 ppm, confirming the presence of both aromatic and aliphatic carbon atoms in the structure (Fig. S5b). Similarly, the ^{1}H NMR spectrum of **MT-C3-D-OH** exhibited aromatic proton signals in the range of 7.09–6.37 ppm and aliphatic proton signals between 4.39 and 2.11 ppm (Fig. S8a). The ^{13}C NMR spectrum displayed sixteen carbon signals between 159.97 and 29.17 ppm, which is consistent with the proposed molecular framework containing aromatic rings and aliphatic chains (Fig. S8b).

The mass spectra further confirmed the molecular structures of the synthesized ligands. The molecular ion peak was observed at *m*/*z* 344.310 $[M + H]^+$ for **MT-C3-H-OH** (Fig. S6) and at *m*/*z* 578.038 $[M]^+$ for **MT-C3-D-OH** (Fig. S9), which are consistent with their expected molecular weights and verify the formation of the target compounds.

The silicon(IV) phthalocyanines **MT-C3-H-Si** and **MT-C3-D-Si** were obtained by reacting the corresponding hydroxyl derivatives with NaH and $SiPcCl_2$ in toluene at 110 °C for 24 h. In the FT-IR spectra, the disappearance of O–H stretching bands confirmed axial substitution. Aromatic C–H stretching vibrations were observed at 3069 cm^{-1} for **MT-C3-H-Si** and 3081 cm^{-1} for **MT-C3-D-Si**, while aliphatic C–H stretching bands appeared at 2964–2855 cm^{-1} and 2960–2860 cm^{-1}, respectively (Fig. S10 and S11).

The ^{1}H NMR spectrum ($CDCl_3$) of **MT-C3-H-Si** exhibited characteristic phthalocyanine macrocycle proton signals. The Pc-H_α and Pc-H_β protons appeared at 9.58 and 8.31 ppm, respectively, which are typical of silicon(IV) phthalocyanine derivatives and confirm the presence of the phthalocyanine core. Additional aromatic proton signals were observed between 7.14 and 5.68 ppm, corresponding to the benzyl aromatic rings introduced through axial substitution, while the aliphatic proton signals resonated in the range of 4.24–2.00 ppm, originating from the morpholine and propyl fragments.

Notably, the Si–O–CH_2 protons were detected at −0.78 ppm. This unusual upfield shift can be attributed to the strong magnetic anisotropy of the phthalocyanine macrocycle, where the ring current effect of the conjugated π-system generates a shielding environment above and below the macrocyclic plane, causing the axial substituent protons located in this region to resonate at negative chemical shift values. This observation further supports the successful axial coordination of the substituents to the silicon center[26] (Fig. 1a). The ^{13}C NMR spectrum displayed aromatic carbon signals between 159.87 and 102.63 ppm, which are attributed to the carbon atoms of the phthalocyanine macrocycle and the aromatic benzyl substituents. In addition, aliphatic carbon signals were observed between 66.85 and 29.10 ppm, corresponding to the carbons of the morpholine and propyl groups introduced through axial substitution (Fig. 1b).

Similarly, **MT-C3-D-Si** exhibited characteristic phthalocyanine macrocycle proton signals, where Pc-H_α and Pc-H_β resonances appeared at 9.57 and 8.27 ppm, respectively. These signals are typical of silicon(IV) phthalocyanine derivatives and confirm the integrity of the phthalocyanine core. Additional aromatic proton signals were observed between 7.18 and 5.50 ppm, corresponding to the aromatic benzyl units attached through axial substitution, while the aliphatic proton signals appearing at 3.85–1.84 ppm were attributed to the morpholine groups and propyl fragments. Similar to the **MT-C3-H-Si** derivative, the Si–O–CH_2 protons were observed at −0.72 ppm due to the strong magnetic anisotropy and ring current effects of the phthalocyanine macrocycle, which create a shielding environment for the axial substituent protons (Fig. 2a). The ^{13}C NMR spectrum revealed fourteen aromatic carbon signals in the range of 159.87–99.20 ppm, corresponding to the carbon atoms of the phthalocyanine macrocycle and the aromatic substituents. In addition, six aliphatic carbon signals were observed between 66.86 and 29.05 ppm, which are assigned to the carbons of the morpholine and propyl chains, further supporting the presence of the axial substituents in the synthesized silicon(IV) phthalocyanine structure (Fig. 2b).

MALDI-TOF MS analysis showed molecular ion peaks at *m*/*z* 1225.105 $[M]^+$ for **MT-C3-H-Si** and 1695.166 $[M]^+$ for **MT-C3-D-Si** (Fig. 3). These molecular ion signals are consistent with the expected molecular weights of the target silicon(IV) phthalocyanine derivatives and provide further confirmation of the axial substitution and formation of the proposed structures.

UV–Vis spectra recorded in DMF indicated that both phthalocyanines predominantly exist in a non-aggregated (monomeric) form, displaying characteristic Q bands at 678 nm for **MT-C3-H-Si** and 681 nm for **MT-C3-D-Si**, together with B (Soret) bands at 332 and 335 nm, respectively (Fig. 4). The presence of sharp and well-defined Q bands suggests that axial substitution with morpholine-containing ligands effectively

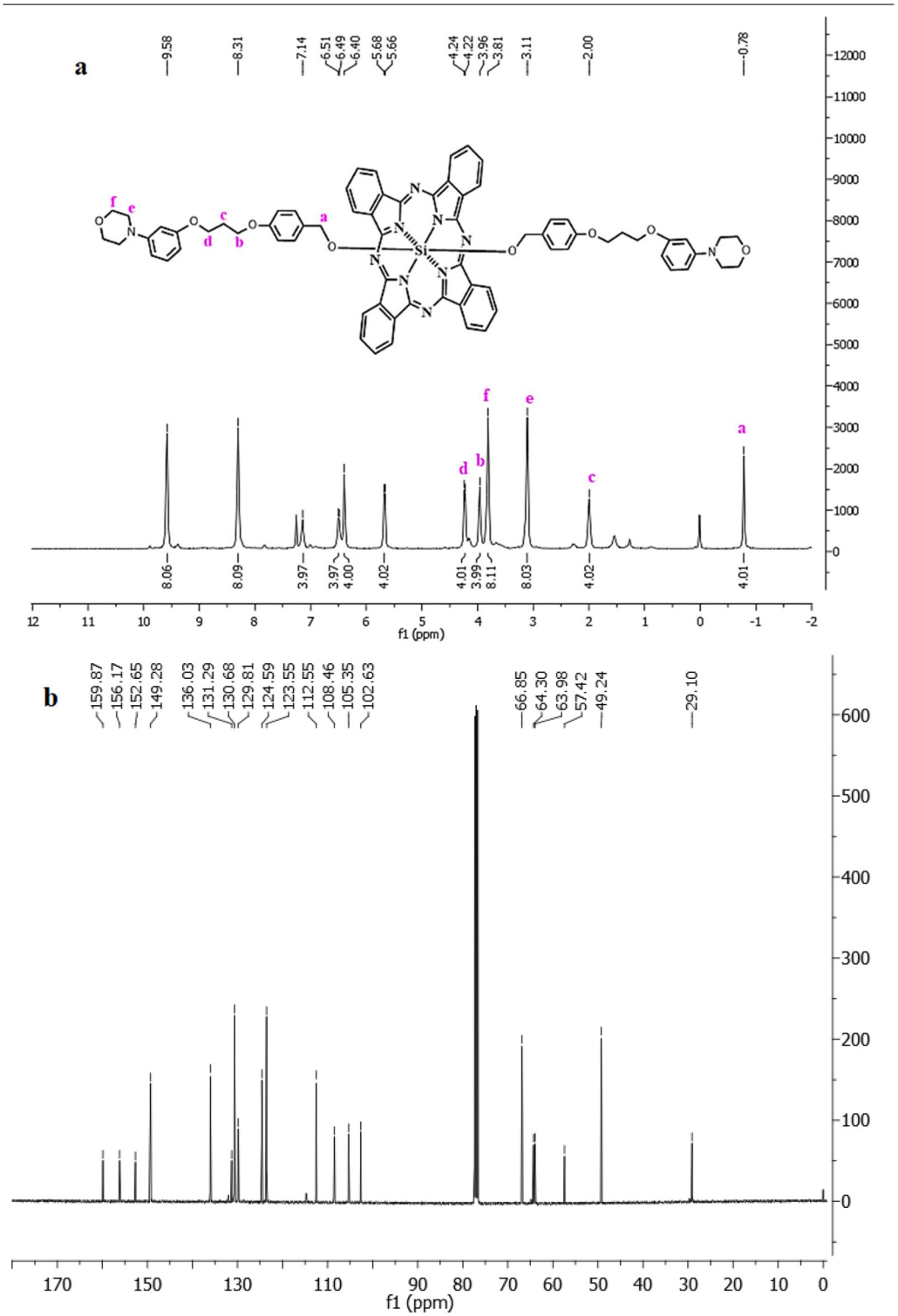

Fig. 1 ^{1}H NMR (a) and ^{13}C NMR (b) spectra of **MT-C3-H-Si** recorded in $CDCl_3$.

suppresses π–π stacking interactions between phthalocyanine macrocycles in DMF, thereby reducing aggregation behavior.

Finally, the water-soluble derivatives **MT-C3-H-SiQ** and **MT-C3-D-SiQ** were synthesized by quaternization of **MT-C3-H-Si** and **MT-C3-D-Si** with iodomethane in chloroform at room temperature. This quaternization reaction converts the tertiary amine groups into quaternary ammonium salts, thereby introducing ionic character and enhancing the solubility of the silicon(IV) phthalocyanine derivatives in polar media. The FT-IR spectra of the quaternized compounds were generally

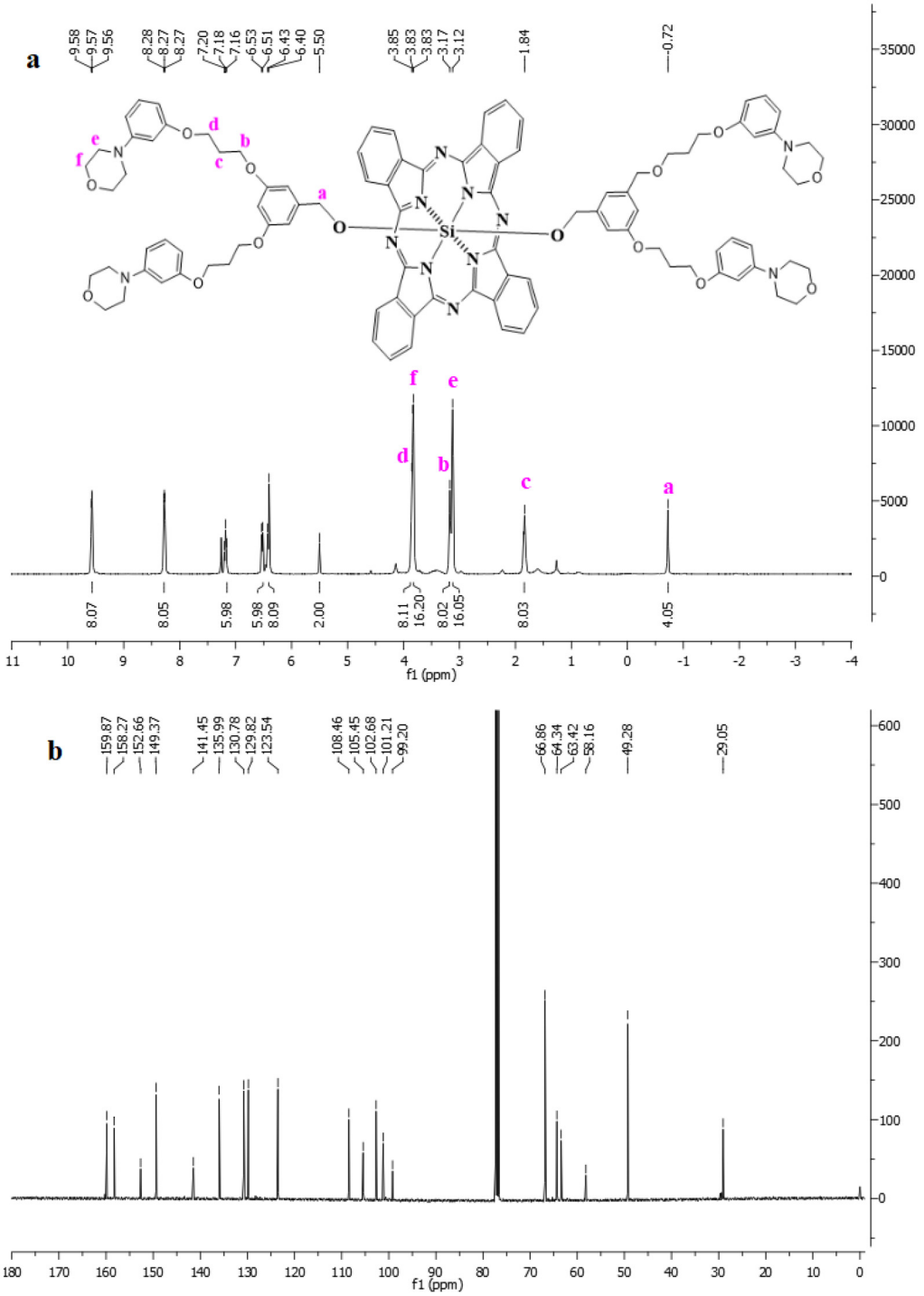

Fig. 2 ^{1}H NMR (a) and ^{13}C NMR (b) spectra of **MT-C3-D-Si** recorded in $CDCl_3$.

similar to those of their non-ionic counterparts, indicating that the phthalocyanine macrocycle and axial substituent framework remained structurally intact after the quaternization process (Fig. S12 and S13). In the UV–Vis spectra recorded in DMF, both **MT-C3-H-SiQ** and **MT-C3-D-SiQ** displayed characteristic Q and B bands at 668 nm and 355 nm, respectively (Fig. 4). Compared with the non-quaternized silicon(IV) phthalocyanines, the water-soluble derivatives exhibited a noticeable shift in the Q-band region, which can be attributed to the electronic influence of the introduced ionic substituents and the resulting changes in the electronic environment of the phthalocyanine macrocycle. In contrast, partial aggregation was observed for the water-soluble derivative **MT-C3-H-SiQ** under the same solvent conditions. This behavior may arise

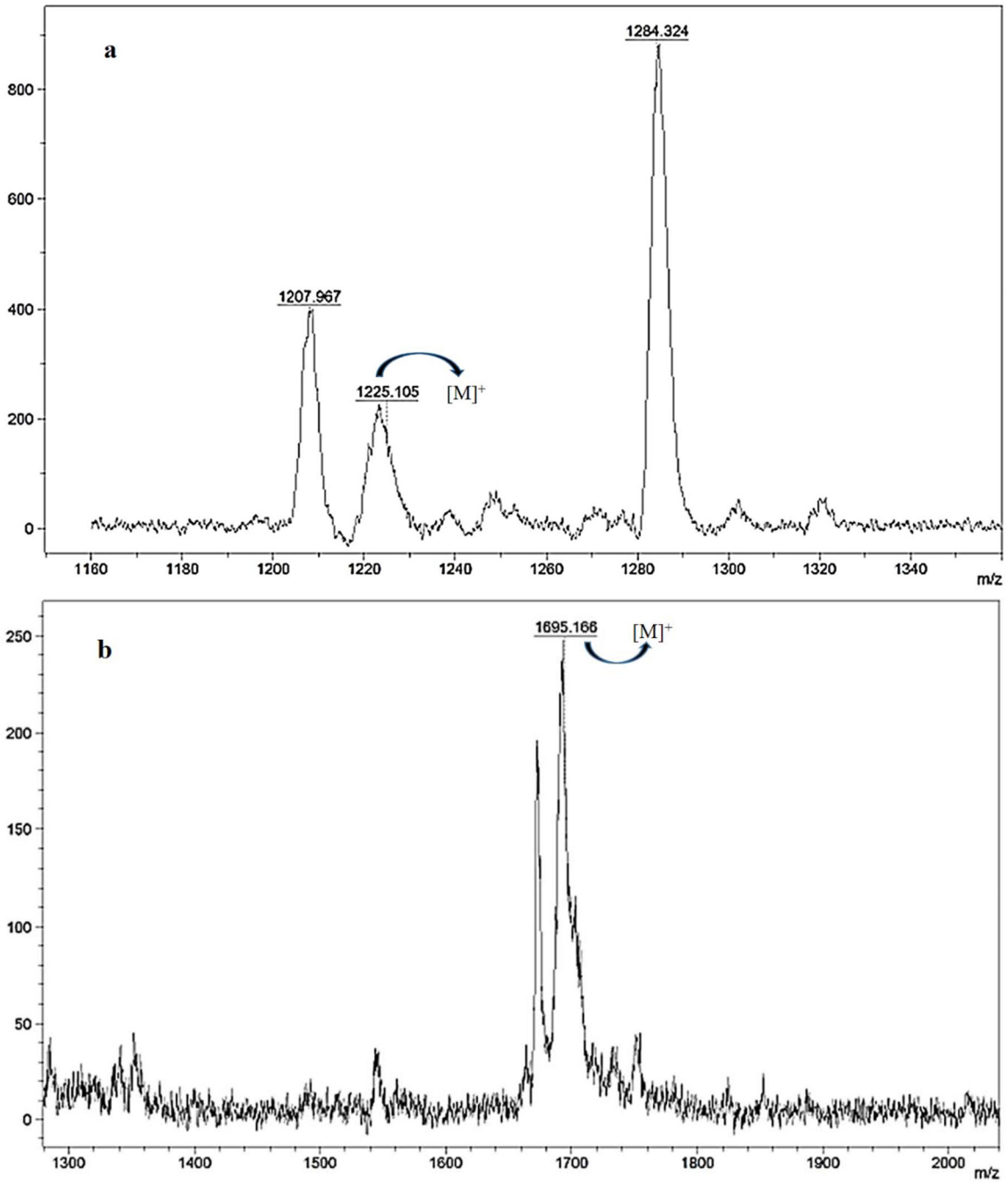

Fig. 3 MALDI–TOF MS spectrum of **MT-C3-H-Si** (a) and **MT-C3-D-Si** (b).

from increased intermolecular interactions associated with the ionic substituents, which can promote aggregation despite the steric effects of axial substitution.[27,28]

The water-soluble derivatives were characterized by MALDI-TOF mass spectrometry using dithranol (DIT) and 3-indoleacrylic acid (IAA) as matrices. For **MT-C3-H-SiQ**, the expected molecular ion was not observed; instead, signals at lower *m*/*z* values (356.563, 556.514, 682.570, 881.249, and 912.496) were detected, which are attributed to fragment ions formed after iodide loss. In particular, the peak at *m*/*z* 682.570 can be assigned to the $[M - 2I + 3H_2O + H]^{2+}$ species, indicating the loss of iodide ions followed by hydration (Fig. 5a). This behavior is consistent with the known ionization characteristics of quaternary ammonium salts under MALDI conditions. For **MT-C3-D-SiQ**, a prominent peak at *m*/*z* 440.849 was observed and assigned to the $M - 4I + H^{4+}$ species, supporting the formation of the tetracationic framework. Additional signals at *m*/*z* 557.495, 577.397, 594.448, and 609.730 were

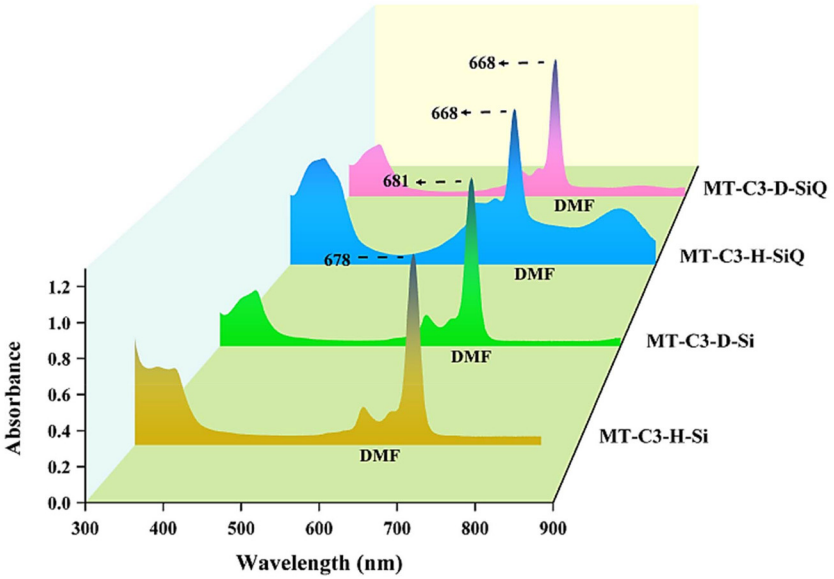

Fig. 4 UV–Vis absorption spectrum of silicon(IV) phthalocyanines recorded in DMF.

attributed to lower charge states and/or partially fragmented species (Fig. 5b). The overall spectral features, including iodide loss, multiply charged ions, and fragmentation patterns, are consistent with the proposed quaternary structures.

3.2. Assays for enzyme inhibition

The α-glycosidase and α-amylase inhibitory activities of the synthesized compounds were evaluated, and the results are summarized in Table 1. Based on the α-glycosidase inhibition data, **MT-C3-H-Si** exhibited the highest inhibitory activity with an IC_{50} value of 16.02 ± 0.94 μM, followed by **MT-C3-D-Si** with an IC_{50} value of 44.14 ± 4.06 μM. The water-soluble derivatives **MT-C3-H-SiQ** and **MT-C3-D-SiQ** showed lower inhibitory activities, with IC_{50} values of 68.80 ± 5.12 μM and >100 μM, respectively. The standard inhibitor acarbose displayed an IC_{50} value of 60.51 ± 4.66 μM. Notably, **MT-C3-H-Si** and **MT-C3-D-Si** demonstrated significantly higher inhibitory activity than acarbose ($p < 0.0001$).

Comparable inhibition trends have been reported in the literature. Çelik *et al.* investigated the α-glycosidase inhibitory activity of silicon(IV) phthalocyanines containing 1,2,3-triazole Schiff base or methoxy homolog substituents and reported that the methoxy-substituted phthalocyanine was approximately 700 times more effective than the standard inhibitor, with an IC_{50} value of 22.4 ± 1.0 μM.[21] Similarly, Barut and Demirbaş evaluated non-peripheral triclosan-substituted metal-free, copper(II), and nickel(II) phthalocyanines and found that the copper(II) derivative exhibited strong α-glycosidase inhibition (IC_{50} = 25.12 ± 0.62 μM), surpassing the other two compounds and the standard inhibitor.[29]

In another study, Khan *et al.* synthesized benzimidazolium salts bearing *N*-methylmorpholine groups and reported α-glycosidase IC_{50} values ranging from 15 ± 0.03 to 110 ± 0.11 μM, with the bromo-substituted derivative identified as the most potent inhibitor (IC_{50} = 15 ± 0.03 μM).[30] Menteşe *et al.* reported even stronger inhibition for certain morpholine derivatives, with IC_{50} values between 0.18 ± 0.021 and 20.46 ± 0.21 μM, and a 4-methoxyphenyl-substituted compound showing approximately 900-fold higher inhibition than the standard inhibitor.[31] Çakmak *et al.* investigated morpholine-substituted quinoline derivatives and reported IC_{50} values between 584.20 ± 62.51 and 1023.16 ± 103.27 μM, which were still higher than that of the standard inhibitor (IC_{50} = 1160.7 ± 172 μM), with the 5-nitro-3,6,8-tribromoquinoline derivative exhibiting the highest inhibition.[32]

Within the present study, **MT-C3-H-Si** and **MT-C3-D-Si** emerged as the most active silicon(IV) phthalocyanines in terms of α-glycosidase inhibition. The presence of morpholine substituents appears to contribute positively to α-glycosidase inhibition, consistent with the previously reported structure–activity relationships. However, literature reports focusing specifically on α-glycosidase inhibition by silicon(IV) phthalocyanines remain limited, and the results of the present study are in agreement with the available findings. Several studies have demonstrated the effectiveness of morpholine-derived compounds as scaffold structures for developing *in vitro* antidiabetic agents.[33] Kayukova and colleagues tested the enzyme inhibitory potential of aroyl-(morpholin-1-yl)propionamidoxime bases and their salts. These compounds inhibited α-glycosidase by 22.8% to 78.7% and α-amylase by 25.6% to 48.0%. They exhibited α-glycosidase inhibitory effects comparable to acarbose, while demonstrating weak α-amylase inhibition.[34] In a different study, Saroha and co-workers examined the *in vitro* amylase inhibitory activity of morpholine-conjugated aurone derivatives. It was found that these compounds exhibited moderate inhibition of α-amylase, ranging from 7.22% to 22.48%.[35]

Regarding α-amylase inhibition, all synthesized compounds exhibited IC_{50} values above 100 μM, indicating weak inhibitory

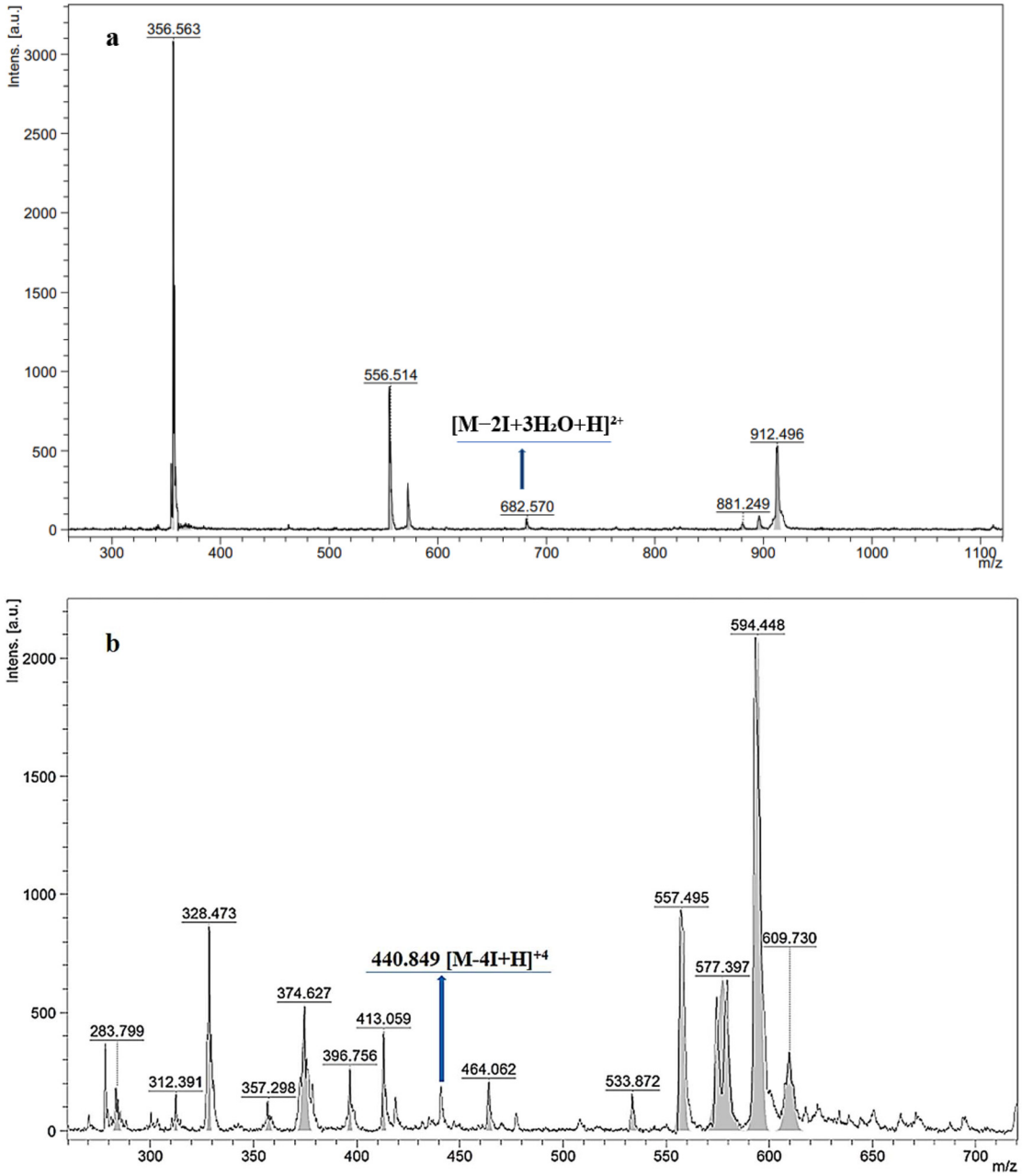

Fig. 5 MALDI–TOF MS spectrum of **MT-C3-H-SiQ** (a) and **MT-C3-D-SiQ** (b).

Table 1 The α-glycosidase and α-amylase inhibitory properties of compounds

Compounds	α-Glycosidase (μM)	α-Amylase (μM)
MT-C3-H-Si	16.02 ± 0.94***	>100
MT-C3-D-Si	44.14 ± 4.06***	>100
MT-C3-H-SiQ	68.80 ± 5.12	>100
MT-C3-D-SiQ	>100	>100
Acarbose	60.51 ± 4.66	25.29 ± 3.50

*** $p < 0.0001$ *vs.* acarbose.

activity, whereas the standard inhibitor acarbose showed an IC_{50} value of 25.29 ± 3.50 μM. This inhibition profile is consistent with the desired pharmacological behavior for Type II diabetes management, where selective α-glycosidase inhibition over α-amylase inhibition is preferred. In a study by Çelik *et al.*, silicon(IV) phthalocyanines displayed IC_{50} values of 78 ± 2 and >400 μM against α-amylase, while acarbose showed an IC_{50} value of 48 ± 2 μM, confirming their weak α-amylase inhibition.[21] Similarly, Saka *et al.* reported low α-amylase inhibition for peripheral copper(II) and zinc(II) phthalocyanines, with IC_{50} values >450 and 128.2 ± 1.5 μM, respectively, compared to the standard inhibitor (IC_{50} = 6.9 ± 0.1 μM).[36]

Additional studies further support this trend. Huneif *et al.* investigated a vanillin–thiazolidinedione–morpholine hybrid compound and reported IC_{50} values of 10.32 ± 1.02 μM for the standard inhibitor and 19.51 ± 1.34 μM for the synthesized compound, indicating lower potency relative to the standard.[37] Likewise, Askarzadeh *et al.* demonstrated that a morpholine-containing phthalimide–benzenesulfonamide derivative showed no α-amylase inhibition at 300 μM, whereas acarbose exhibited an IC_{50} value of 108 ± 0.71 μM.[38]

The water-soluble silicon(IV) phthalocyanines (**MT-C3-H-SiQ** and **MT-C3-D-SiQ**) displayed lower inhibitory activity against both α-glycosidase and α-amylase compared to their non-ionic counterparts (**MT-C3-H-Si** and **MT-C3-D-Si**). This observation suggests that increased hydrophilicity and quaternization may adversely affect enzyme–inhibitor interactions. Enhanced water solubility does not necessarily translate into improved enzyme inhibition, highlighting the importance of maintaining an optimal balance between aqueous solubility and biological activity during inhibitor design. The fact that the *in vitro* α-amylase inhibitory activity of morpholine derivatives remains at a low to moderate level highlights the need for structural modifications to enhance their efficacy. On the other hand, studies investigating the antidiabetic potential of morpholine-substituted phthalocyanine compounds are quite limited in the literature. Notably, investigations focusing on axially disubstituted and water-soluble silicon(IV) phthalocyanines remain scarce. Therefore, this work provides valuable insight by systematically evaluating both α-glycosidase and α-amylase inhibition, supported by kinetic analysis, within a single silicon(IV) phthalocyanine framework, thereby contributing to an existing gap in the literature.

Table 2 Kinetic analyses of **MT-C3-H-Si** and **MT-C3-D-Si** against α-glycosidase

Compounds	Type	K_i (μM)
MT-C3-H-Si	Non-competitive	9.45 ± 1.45
MT-C3-D-Si	Non-competitive	29.06 ± 5.16

3.3. Kinetic analyses of compounds

The inhibition mechanism and inhibition constants (K_i) of **MT-C3-H-Si** and **MT-C3-D-Si**, which exhibited the highest inhibitory activity against α-glucosidase, were investigated through enzyme kinetic analysis. The kinetic parameters obtained are summarized in Table 2.

As shown in Fig. 6, the presence of **MT-C3-H-Si** led to a decrease in the V_{max} value, while the K_m value remained unchanged. This kinetic behavior indicates that **MT-C3-H-Si** inhibits α-glucosidase *via* a non-competitive inhibition mechanism. The inhibition constant for **MT-C3-H-Si** was calculated as 9.45 ± 1.45 μM.

Similarly, as illustrated in Fig. 7, the addition of **MT-C3-D-Si** resulted in a reduction of the V_m value without affecting the K_m value, demonstrating a non-competitive inhibition pattern toward α-glucosidase. The calculated K_i value for **MT-C3-D-Si** was 29.06 ± 5.16 μM, indicating a lower binding affinity compared to **MT-C3-H-Si**.

The kinetic evaluation of **MT-C3-H-Si** and **MT-C3-D-Si** provided important insights into the inhibition behavior of these silicon(IV) phthalocyanines toward α-glucosidase. The observed decrease in V_{max} without a significant change in K_m values clearly indicates a non-competitive inhibition mechanism, suggesting that both compounds interact with the enzyme at a site distinct from the active site. This behavior implies that enzyme inhibition is not directly influenced by substrate concentration and cannot be overcome by increasing substrate levels.

The non-competitive inhibition profile observed for **MT-C3-H-Si** and **MT-C3-D-Si** may be attributed to the structural features of axially disubstituted silicon(IV) phthalocyanines. The rigid macrocyclic framework and axial substitution pattern are likely to facilitate interactions with allosteric regions of the enzyme, leading to conformational changes that reduce cata-

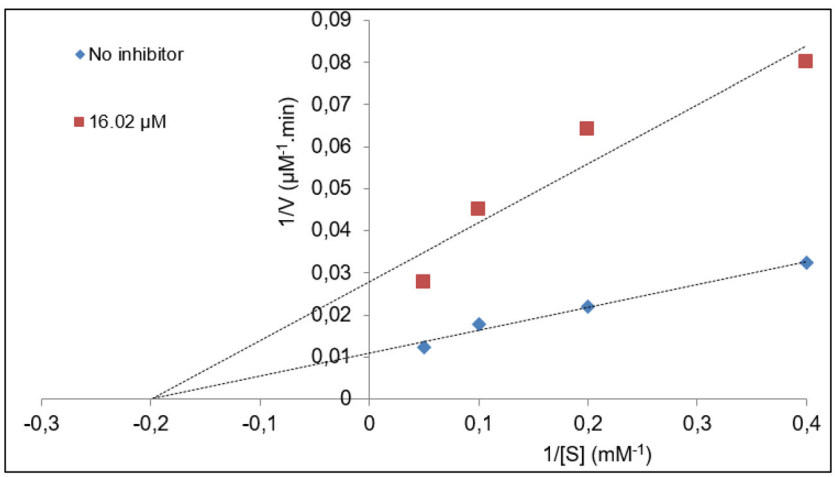

Fig. 6 Lineweaver–Burk graph of **MT-C3-H-Si** on α-glycosidase.

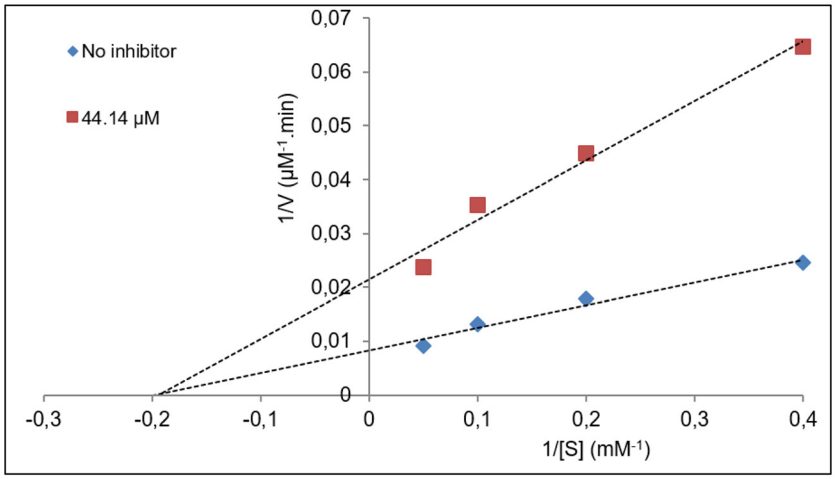

Fig. 7 Lineweaver–Burk graph of **MT-C3-D-Si** on α-glycosidase.

lytic efficiency. Such an inhibition mechanism is particularly advantageous for therapeutic applications, as it may provide more consistent enzyme inhibition under varying physiological substrate concentrations.[39]

Comparison of the inhibition constants further reveals that **MT-C3-H-Si** exhibits a stronger affinity toward α-glycosidase than **MT-C3-D-Si**, as evidenced by its lower K_i value. This difference may be associated with variations in the axial substituent architecture, which can influence molecular flexibility, steric accessibility, and the overall interaction strength with the enzyme surface.[40,41] These findings suggest that subtle modifications in axial functionalization play a critical role in modulating enzyme–inhibitor interactions.

From a pharmacological perspective, the combination of strong α-glucosidase inhibition, limited α-amylase inhibition, and a non-competitive inhibition mechanism is highly desirable for the management of Type 2 diabetes.[42] This inhibition profile may help reduce postprandial glucose levels while minimizing gastrointestinal side effects commonly associated with strong α-amylase inhibition. Overall, the kinetic behavior of the synthesized silicon(IV) phthalocyanines supports their potential as promising candidates for further development as antidiabetic agents.

4. Conclusion

In this study, a series of axially disubstituted silicon(IV) phthalocyanines and water-soluble derivatives were synthesized and comprehensively characterized using spectroscopic techniques. The *in vitro* biological evaluation demonstrated that selected silicon(IV) phthalocyanines exhibited significant inhibitory activity against α-glycosidase while showing comparatively weak inhibition toward α-amylase. This selective inhibition profile is considered advantageous for the management of Type 2 DM, as strong α-glycosidase inhibition combined with limited α-amylase inhibition may help reduce postprandial hyperglycemia while minimizing gastrointestinal side effects. Enzyme kinetic studies revealed that the most active compounds, **MT-C3-H-Si** and **MT-C3-D-Si**, inhibited α-glycosidase through a non-competitive mechanism. Overall, the results of this study highlight that the combination of selective enzyme inhibition and a non-competitive inhibition mechanism underscores the potential of these compounds for further pharmacological investigation. Future studies focusing on structure optimization, *in silico* modeling, and advanced biological evaluations may further clarify the therapeutic potential of this class of compounds in Type 2 DM management.

Author contributions

Turgut Keleş: investigation, methodology, and data curation. Zekeriya Biyiklioglu: conceptualization, supervision, and writing – review & editing. Gökçe Seyhan: investigation, data curation, and formal analysis. Burak Barut: formal analysis and writing – original draft.

Conflicts of interest

There are no conflicts to declare.

Data availability

The data supporting this article have been included as part of the supplementary information (SI). Supplementary file includes raw data, additional figures, and statistical analysis details. See DOI: https://doi.org/10.1039/d6dt00405a.

Acknowledgements

This work was supported by the Scientific and Technological Research Council of Turkey (TÜBİTAK) under Project No. 124Z983.

References

1 A. Poznyak, A. V. Grechko, P. Poggio, V. A. Myasoedova, V. Alfieri and A. N. Orekhov, *Int. J. Mol. Sci.*, 2020, **21**, 1–13.
2 M. Su, T. Tang, W. Tang, Y. Long, L. Wang and M. Liu, *Front. Immunol.*, 2023, **14**, 1–12.
3 W. Mi, Y. Xia and Y. Bian, *Inflammation Res.*, 2019, **68**, 275–284.
4 M. J. Hossain, M. Al-Mamun and M. R. Islam, *Health Sci. Rep.*, 2024, **7**, 5–9.
5 X. Cheng, J. Huang, H. Li, D. Zhao, Z. Liu, L. Zhu, Z. Zhang and W. Peng, *Phytomedicine*, 2024, **126**, 154887.
6 C. Ge, Z. Shi, J. He, X. Feng, K. Shang, X. Liao, Y. Liu, Y. Jiang and S. Liu, *Pharm. Biol.*, 2026, **64**, 130–142.
7 L. Zhao, S. Luo, Z. Peng and G. Wang, *Int. J. Biol. Macromol.*, 2025, **302**, 140637.
8 T. S. Chaithanya and V. Sabareesh, *Pept. Sci.*, 2025, DOI: 10.1002/pep2.70017.
9 G. Wu, W. He, H. Rao, L. Lu, X. He and X. Hou, *Front. Endocrinol. (Lausanne).*, 2025, **16**, 1–8.
10 F. Khan, S. Ahmad, K. Osama, A. Farooqui, A. Kumar and S. Akhtar, *Mol. Divers.*, 2025, DOI: 10.1007/s11030-025-11307-2.
11 Y. C. Feng, X. Wang and D. Wang, *Mater. Chem. Front.*, 2023, **8**, 228–247.
12 H. Y. Yenilmez, Ö. Budak, N. F. Öztürk, A. Koca, A. Boz, B. Ustamehmetoğlu and Z. Altuntaş Bayır, *Dalton Trans.*, 2023, **53**, 1766–1778.
13 Ö. Güleç, A. T. Bilgiçli, C. Hepokur, A. Günsel, M. Arslan and M. Nilüfer Yarasir, *J. Photochem. Photobiol., A*, 2024, **452**, 115587.
14 G. Zanotti, P. Imperatori, A. M. Paoletti and G. Pennesi, *Molecules*, 2021, DOI: 10.3390/molecules26061760.
15 V. T. Verdree, S. Pakhomov, G. Su, M. W. Allen, A. C. Countryman, R. P. Hammer and S. A. Soper, *J. Fluoresc.*, 2007, **17**, 547–563.
16 S. Ünlü, Z. Köksal, K. Kübra Kırboğa and F. T. Elmalı, *J. Mol. Struct.*, 2026, **1353**, 144615.
17 H. Messaoudi, G. Yaşa Atmaca and A. Erdoğmuş, *J. Mol. Struct.*, 2024, **1312**, 138394.
18 P. Saha, S. Das, H. K. Indurthi and D. K. Sharma, *Dyes Pigm.*, 2022, **206**, 110608.
19 D. Li, S. Cai, P. Wang, H. Cheng, B. Cheng, Y. Zhang and G. Liu, *Adv. Healthcare Mater.*, 2023, **12**, 1–24.
20 D. Güngördü Solğun, S. Özdemir, A. Dündar and M. S. Ağırtaş, *J. Photochem. Photobiol., A*, 2024, **456**, 115794.
21 F. Çelik, Y. Ünver, F. OzTuncay, U. Cakmak, Y. Kolcuoglu, K. K. Uzun, H. Ozturk, N. Yorulmaz and İ. Değirmencioğlu, *J. Organomet. Chem.*, 2024, **1016**, 123237.
22 H. Yalazan, B. Barut, C. Ö. Yalçın, H. Kantekin and S. Yıldırmış, *Inorg. Chem. Commun.*, 2024, **165**, 112548.
23 H. O. Gulcan, S. Unlu, I. Esiringu, T. Ercetin, Y. Sahin, D. Oz and M. F. Sahin, *Bioorg. Med. Chem.*, 2014, **22**, 5141–5154.
24 H. Nara, A. Kaieda, K. Sato, T. Naito, H. Mototani, H. Oki, Y. Yamamoto, H. Kuno, T. Santou, N. Kanzaki, J. Terauchi, O. Uchikawa and M. Kori, *J. Med. Chem.*, 2017, **60**, 608–626.
25 K. K. Palaniappan, A. A. Pitcher, B. P. Smart, D. R. Spiciarich, A. T. Iavarone and C. R. Bertozzi, *ACS Chem. Biol.*, 2011, **6**, 829–836.
26 T. Keles, G. Seyhan, Z. Biyiklioglu, K. Kolci, R. Reis and B. Barut, *Appl. Organomet. Chem.*, 2024, **38**, 2–9.
27 G. De La Torre, C. G. Claessens and T. Torres, *Chem. Commun.*, 2007, 2000–2015.
28 T. Nyokong, *Coord. Chem. Rev.*, 2007, **251**, 1707–1722.
29 B. Barut and Ü. Demirbaş, *J. Organomet. Chem.*, 2020, **923**, 121423.
30 I. A. Khan, F. A. Saddique, S. Aslam, U. A. Ashfaq, M. Ahmad, S. A. Al-Hussain and M. E. A. Zaki, *Molecules*, 2022, **27**, 1–13.
31 E. Menteşe, N. Baltaş and M. Emirik, *Bioorg. Chem.*, 2020, **101**, 104002.
32 O. Çakmak, S. Ökten, D. Alımlı, C. C. Ersanlı, P. Taslimi and Ü. M. Koçyiğit, *J. Mol. Struct.*, 2020, **1220**, 128666.
33 D. Zolotareva, A. Zazybin, A. Dauletbakov, Y. Belyankova, B. Giner Parache, S. Tursynbek, T. Seilkhanov and A. Kairullinova, *Molecules*, 2024, **29**, 3043.
34 L. A. Kayukova, A. B. Uzakova, G. P. Baitursynova, G. T. Dyusembaeva, Z. T. Shul'gau, A. E. Gulyaev and S. D. Sergazy, *Pharm. Chem. J.*, 2019, **53**, 129–133.
35 B. Saroha, G. Kumar, P. Arya, N. Raghav and S. Kumar, *Bioorg. Chem.*, 2023, **140**, 106805.
36 E. Tugba Saka, U. Cakmak, C. Akkol and Z. Biyiklioglu, *Polyhedron*, 2023, **243**, 116522.
37 M. A. Huneif, D. B. Alshehri, K. S. Alshaibari, M. Z. Dammaj, M. H. Mahnashi, S. U. Majid, M. A. Javed, S. Ahmad, U. Rashid and A. Sadiq, *Biomed. Pharmacother.*, 2022, **150**, 113038.
38 M. Askarzadeh, H. Azizian, M. Adib, M. Mohammadi-Khanaposhtani, S. Mojtabavi, M. A. Faramarzi, S. M. Sajjadi-Jazi, B. Larijani, H. Hamedifar and M. Mahdavi, *Sci. Rep.*, 2022, **12**, 1–16.
39 S. N. Meena, U. Kumar, M. M. Naik, S. C. Ghadi and S. G. Tilve, *Bioorg. Med. Chem.*, 2019, **27**, 2340–2344.
40 E. Güzel, B. S. Arslan, K. Çlkrlkçl, A. Ergün, N. Gençer, O. Arslan, I. Şişman and M. Nebioğlu, *J. Porphyrins Phthalocyanines*, 2020, **24**, 1047–1053.
41 T. Keleş, Z. Biyiklioglu, E. Gültekin and O. Bekircan, *Inorg. Chim. Acta*, 2019, **487**, 201–207.
42 S. Rocha, A. Sousa, D. Ribeiro, C. M. Correia, V. L. M. Silva, C. M. M. Santos, A. M. S. Silva, A. N. Araújo, E. Fernandes and M. Freitas, *Food Funct.*, 2019, **10**, 5510–5520.